Title page

A molecularly distinct cell type in the midbrain regulates intermale aggression behaviors in mice

Chun-Yang Li[1,2,3,8], Cheng Miao[2,3,8], Yao Ge[3,4,5], Jiaxing Wu[2,3], Panpan Gao[2,3], Songlin Yin[2,3], Pei Zhang[3,4], Bo Tian[3,4], Wenqiang Chen[6,7]*, Xiao-Qian Chen[2,3]*

[1]Advanced Medical Research Central of Zhengzhou University, Zhengzhou Central Hospital Affiliated to Zhengzhou University, Zhengzhou, 450007, China. [2]Department of Pathophysiology, School of Basic Medicine, Tongji Medical College, Huazhong University of Science and Technology, Wuhan 430030, China. [3]Key Laboratory of Neurological Diseases, Ministry of Education, Wuhan, Hubei Province, 430030, China. [4]Department of Neurobiology, School of Basic Medicine, Tongji Medical College, Huazhong University of Science and Technology, Wuhan 430030, China. [5]Key Laboratory of Developmental Genes and Human Disease, School of Life Science and Technology. Southeast University, Nanjing 210096, China. [6]Section of Integrative Physiology and Metabolism, Joslin Diabetes Center and Department of Medicine, Harvard Medical School, Boston, MA 02215, USA. [7]Translational Medicine, Steno Diabetes Center Copenhagen, Herlev, 2730, Denmark. [8]These authors contributed equally.

***Corresponding authors**: Xiao-Qian Chen; Wenqiang Chen
Email: chenxq@mails.tjmu.edu.cn (X.Q. Chen); Wenqiang.chen@joslin.harvard.edu (W. Chen)
Lead contact: chenxq@mails.tjmu.edu.cn (X.Q. Chen)

Running title:
dmPAG cells regulate aggression

Keywords:
Periaqueductal gray, Tachykinin, Aggression, Translating ribosome affinity purification, Chemogenetics, Serotonin

NOTE: this is a revised version of the previous biorxiv submission:
doi: https://doi.org/10.1101/2023.10.19.562724

ACKNOWLEDGEMENT:
This work was funded by National Natural Science Foundation of China (No. 82173197 and 81972362) to X.Q.C. The authors thank Prof. Minmin Luo for kindly providing *Tac2*-Cre knock-in mouse line, Prof. Jian-Zhi Wang for kindly providing Ai9/tdTomato mice, and Prof. Yunyun Han for kindly providing suggestions on Ca^{2+} imaging. The authors gratefully thank the members from the X.Q. Chen Lab help with this project during the first-wave of COVID-19 in Wuhan.

AUTHOR CONTRIBUTIONS:
C.Y.L. researched, analyzed, interpretated data, and helped write the manuscript. C.M., J.W., Y.G., P.G., S.Y., P.Z., and B.T. researched data and helped analyze data. W.C. conceived and designed the study, interpretated data and wrote the manuscript; X.Q.C. secured the funding, designed the study, interpretated data, supervised all work and helped write the manuscript.

DISCLOSURES:
The authors declare no competing interests.

ABSTRACT

BACKGROUND: The periaqueductal gray (PAG) is a central hub for regulation of aggression, whereas little is known on the circuitry and molecular mechanisms that govern this regulation. We investigate the role of a distinct cell type, *Taschykinin 2*-expressing ($Tac2^+$) neurons, located in the dorsomedial PAG (dmPAG), in modulating aggression in mice.

METHODS: We combined activity mapping, *in vivo* Ca^{2+} recording, chemogenetic and pharmacological manipulation, and a viral-based translating ribosome affinity purification (TRAP) profiling using a mouse resident-intruder model.

RESULTS: We demonstrate that the $dmPAG^{Tac2}$ neurons were exclusively activated by fighting behaviors. Further, we show that activation of the $dmPAG^{Tac2}$ neurons evoked, while inhibition or genetic ablation of the $dmPAG^{Tac2}$ neurons suppressed fighting behaviors. TRAP proofing of $dmPAG^{Tac2}$ neurons revealed that fighting behaviors specifically induced enrichment of serotonin-associated transcripts to the $dmPAG^{Tac2}$ neurons. Last, we validated these findings by selectively delivering pharmacological agents into the dmPAG and reversed the behavioral outcomes induced by chemogenetic manipulation.

CONCLUSIONS: We identify that the $dmPAG^{Tac2}$ neuron can regulate mouse aggressive behavior and thus suggest a distinct molecular target for the treatment of exacerbated aggressive behavior in populations that exhibit high-level of violence.

INTRODUCTION

The periaqueductal gray (PAG) is a conserved brain region located in the midbrain traditionally viewed as a key integration center for processing upstream information related to emotion (Chen et al., 2018; Motta et al., 2017; Silva and McNaughton, 2019). Early studies have demonstrated that electrical stimulation of the PAG in cats directly elicited an aggressive-defensive response, while lesions of the PAG blocked this response (Hunsperger, 1956; Hunsperger and Bucher, 1967). Electrical stimulation of the amygdala and the hypothalamus also induced aggressive responses, however, when these regions are lesioned, PAG stimulation still elicited robust aversive responses (Schreiner and Kling, 1953), suggesting that the PAG may play an independent role in eliciting aversive responses such as aggression.

Functional activity-dependent studies also confirmed the critical roles of the PAG in regulating aggression and defense behaviors. More recently, studies using optogenetics, Ca^{2+} imaging, and electrophysiological recording of the PAG have revealed the causal roles of the PAG in aggressive and defensive behaviors. Of note, many of these studies were conducted in subregions such as the dorsal PAG (dPAG) and the lateral PAG (lPAG) in a pan-neuronal manner (Deng et al., 2016; Lischinsky and Lin, 2020). However, there is a lack of understanding of whether an anatomically and molecularly distinct cell type in the PAG that might regulate aggressive behaviors.

In recent years, the crucial role of Tac2 positive ($Tac2^+$) neurons in emotional behavior regulation has been revealed, including fear memory and social behaviors (Andero et al., 2014; Zelikowsky et al., 2018). In this study, we focused on $Tac2^+$ neurons in the midbrain, specifically in the dorsomedial part of the PAG (dmPAG). Using a resident-intruder (RI) paradigm in mice, we revealed a critical role of $dmPAG^{Tac2}$ neurons in aggression. Further, we explore the possible molecular targets in $dmPAG^{Tac2}$ neurons through a TRAP-seq profiling and pharmacological agent-based validation. Collectively, these findings show that the *Tac2*-expressing neurons serve as a molecularly distinct cell type in the PAG that regulates intermale aggression and thus suggesting that targeting these cells might help alleviate symptoms in humans exhibiting high levels of aggression and violence.

RESULTS

Tac2-expressing neurons exhibit distinct expression pattern in the PAG

Previous studies reported that $Tac2^+$ neurons are expressed in a wide range of brain areas including the amygdala, hypothalamus, nucleus accumbens (Mar et al., 2012), however, their expression pattern in the PAG has not been characterized. To this end, we crossed *Tac2*-Cre knock-in mice with Ai9 reporter mice to selectively express a tdTomato in $Tac2^+$ cells (**Figure 1A**). By aligning expression of $Tac2^{tdTomato}$ cells to the Allen Brain Atlas (ABA), we confirmed that $Tac2^{tdTomato}$ cells were located in selected brain areas such as the hypothalamus and amygdala (**Figure 1B-C**), consistent with previous reports (Mar et al., 2012; Zelikowsky et al., 2018). No $tdTomato^+$ cells were found in control mice including the *Tac2*-Cre mice, Ai9 mice, and wide-type mice (**Figure S1A**).

We then specifically analyzed the expression pattern in the PAG. $Tac2^{tdTomato}$ cells were expressed throughout the PAG (**Figure 1D**), consistent with the mRNA expression pattern noted in the ABA (**Figure S1B**). $Tac2^{tdTomato}$ cells were primarily located in the dmPAG (**Figure 1E-F**), to a level of 50% of the total numbers of *Tac2*-expressing cells in the pan-PAG areas. Similarly, *Tac2* mRNAs were predominantly expressed in the dmPAG (54.4%, **Figure S1C-D**). Thus, these data establish that the PAG *Tac2*-expressing cells are mainly located in the dorsomedial subregion.

dmPAG^{Tac2} neurons respond to aggression

We next sought to determine the involvement of the dmPAG^{Tac2} neurons in fighting behaviors. First, we subjected the WT mice to a RI assay and harvested brain tissues after fighting (**Figure 2A**). As expected, fighting behaviors activated neurons in a broad range of brain areas, including the paraventricular nucleus of the thalamus, periventricular zone, anterior hypothalamic nucleus (**Figure S2**). Focusing on the c-Fos^{+} neurons in the dmPAG, our results showed that, compared to the control mice kept at home cages, a significant number of c-Fos^{+} neurons were found in the dmPAG of the resident mice (**Figure 2B-C**). In contrast, fighting behaviors had minimal effects in inducing c-Fos expression in other PAG subregions, such as the dlPAG, lPAG, and vlPAG (**Figure S2B-C**).

We then investigated the role of dmPAG neurons in response to fighting behaviors using an *in vivo* fiber photometry. AAV vector carrying GCaMP6m was injected into the dmPAG of WT mice and then a fiber was implanted above the dmPAG (**Figure 2D**). Correct placement of the fiber was verified (**Figure 2E**). When subjected these mice to the RI, we observed a large increase in Ca^{2+} transients in response to each attack bouts (**Figure 2F-G**). Notably, each attack elicited an increase in Ca^{2+} activity immediately after the start of the attack episodes and this increase returned to baseline level after an attack (**Figure 2H**). Thus, these results demonstrated the involvement of dmPAG neurons in fighting behaviors.

We further investigated the role of dmPAG^{Tac2} neurons in fighting behaviors. We used a Cre-dependent AAV vector (**Figure 3A**) to label dmPAG^{Tac2} neurons and then subjected the mice to the RI (**Figure 3B**). Staining c-Fos proteins in mCherry^{+} cells confirmed that dmPAG^{Tac2} neurons were activated by fighting behaviors (**Figure 3C**). We then measured Ca^{2+} activity of dmPAG^{Tac2} neurons during the RI by injecting a Cre-dependent AAV vector carrying GCaMP6m (**Figure 3D-E**) and verified the correct placement of the optic fiber (**Figure 3F**). We observed an increase in Ca^{2+} activity in response to attack episode (**Figure 3G-I**). We correlated each component of an attack event to Ca^{2+} activity (**Figure 3G**) and found that attacks reliably induced Ca^{2+} transient, but none of the other attack-associated events (tail rattling, sniffing, and grooming) could significantly alter Ca^{2+} activity (**Figure 3J-O**). In addition, using a Cre-out strategy, we revealed that dmPAG Tac2-negative neurons showed a mild but a significant increase in Ca^{2+} activity following each attack episode ($P<0.05$, **Figure S3A-D**). This increase was, however, three times lower than that of the dmPAG^{Tac2} neurons ($P<0.0001$, **Figure S3E-F**), suggesting that, while the other cell types in the dmPAG might contribute, at least partially, to the fighting behaviors, consider the degrees of increase in Ca^{2+} activity (**Figure 3I** and **Figure S3D-F**), the dmPAG^{Tac2} neurons still exhibited a dominant role in response to aggression.

The PAG is a highly heterogenous region and is involved in many functions, including sensorimotor function and pain sensation (Carrive, 1993; Silva and McNaughton, 2019). To further test the specificity of dmPAG^{Tac2} neurons in fighting behaviors, we subjected these mice to a variety of stimuli and recorded Ca^{2+} activity. The results showed that, dmPAG^{Tac2} neurons failed to exhibit significant altered Ca^{2+} activity in response to male-male and male-female encounter (**Figure S4A-F**), rotarod activity (**Figure S4G-H**), object exploration (**Figure S4I-J**), fox odor sniffing (**Figure S4K-L**), saline sniffing (**Figure S4M-N**), and pain stimulation (**Figure S4O-P**). Thus, these data collectively demonstrated that, the dmPAG^{Tac2} neurons respond specifically to fighting behaviors.

Deletion or inhibition of dmPAG^{Tac2} neurons attenuates fighting behaviors

To further confirm that dmPAG^{Tac2} neurons respond to fighting behaviors, we performed chemogenetic manipulations to examine a causal role of dmPAG^{Tac2} neurons in aggression. First, we performed a basic behavioral characterization of *Tac2*-Cre mice and their WT littermate controls. The results

showed that *Tac2*-Cre mice exhibited similar levels of locomotor performances (**Figure S5A-E**). However, *Tac2*-Cre mice had mild but significantly increased levels of anxiety (**Figure S5F-J**). In addition, *Tac2*-Cre mice exhibited no difference in social preference (**Figure S5K-P**) and notably, *Tac2*-Cre mice had similar levels of fighting behaviors in the RI (**Figure S5Q-T**), which establishes a non-different baseline level of fighting behaviors prior to our next genetic ablation and chemogenetic manipulation experiments.

We then examined the behavioral effects of genetic ablation of dmPAG^{Tac2} neurons by injecting a neuron-specific Cre-dependent AAV encoding DTA-mCherry (**Figure 4A-B**) into the dmPAG of *Tac2*-Cre mice (*Tac2*^{DTA}). *Tac2*-Cre mice injected with a Cre-dependent AAV-mCherry (**Figure 4A-B**) served as the control (*Tac2*^{mCherry}). DTA-mediated ablation resulted in an 80% of ablation of dmPAG^{Tac2} neurons (**Figure 4C-D**), demonstrating high efficiency in ablating *Tac2*-expressing cells in the dmPAG. *Tac2*^{mCherry} mice showed similar level of aggression before and after AAV injection, however, mice with genetic ablation of dmPAG^{Tac2} neurons exhibited a significantly decreased level of aggression (**Figure 4E-G**), when compared not only to the baseline levels (**Figure 4B**), but also to their *Tac2*^{mCherry} control mice. In addition, ablation of the dmPAG^{Tac2} neurons significantly reduced the percentage of mice that exhibited fighting behaviors (**Figure S6A**), whereas this manipulation failed to alter male-male investigation during the encounter (**Figure S6B**). Thus, these data suggest that ablation of dmPAG^{Tac2} neurons attenuates aggression.

Similarly, we performed chemogenetic silencing of dmPAG^{Tac2} neurons. First, AAV with Cre-dependent inhibitory DREADDs vector (hM4Di-mCherry) was injected into the dmPAG of *Tac2*-Cre mice (**Figure 4H-I**, *Tac2*^{hM4Di} mice). *Tac2*-Cre mice injected with a Cre-dependent AAV encoding mCherry construct served as the control (*Tac2*^{mCherry}). We established a baseline level of aggression by administering *Tac2*-Cre mice with normal saline for 30 minutes, followed by the RI test (**Figure 4J**). Forty-eight hours later, these mice were administered with clozapine-N-oxide (CNO, 1 mg/kg, i.p.) and subjected to the RI again. As expected, saline administration failed to alter fighting behaviors in *Tac2*^{mCherry} mice (**Figure 4K-N**), however, the previously established fighting behaviors in the baseline test were dramatically suppressed by CNO administration in *Tac2*^{hM4Di} mice (**Figure 4L-N**). Also, inhibition of dmPAG^{Tac2} neurons significantly reduced the percentage of mice exhibiting fighting behaviors (**Figure S6C**). Of note, we chose to achieve chemogenetic inhibition using a relatively low dose of CNO (1 mg/kg) based on a previous report showing that CNO at higher doses (5 mg/kg) could elicit non-specific response in the absence of the DREADDs receptor expression (MacLaren et al., 2016). Indeed, we did not observe that chemogenetic inhibition of dmPAG^{Tac2} neuronal activity at the dose of 1 mg/kg had any obvious effects in altering locomotion (**Figure S7A-D**), whereas in the elevated-plus maze test, except for an increase of time spent in the open arms (**Figure S7F**, see *Discussion*) after CNO administration, other measures for anxiety-like behaviors exhibited similar levels (**Figure S7E, G-H**). In summary, above results suggest that ablation or inhibition of dmPAG^{Tac2} neurons can reduce aggression behaviors in mice.

Activation of dmPAG^{Tac2} neurons elicits fighting behaviors

Having confirmed the necessity of dmPAG^{Tac2} neurons in fighting behaviors from either ablation or inhibition of these cells, we then performed chemogenetic activation experiment to test the sufficiency of dmPAG^{Tac2} neurons in fighting behaviors. We expressed a neuron-specific Cre-dependent AAV encoding hM3Dq in the dmPAG of *Tac2*-Cre mice (**Figure 5A-B**, *Tac2*^{hM3Dq} mice). *Tac2*-Cre mice receiving AAV-mCherry injection served as the control (**Figure 5A-B**, *Tac2*^{mCherry}). To confirm the efficacy and specificity of chemogenetic activation of dmPAG^{Tac2} neurons, CNO was administered (0.5 mg/kg, i.p.) to examine c-Fos induction in Tac2^{+} cells (**Figure 5C**). The results revealed that c-Fos induction was specific to hM3Dq-expressing neurons but not to mCherry-expressing neurons (**Figure**

5C-D).

Next, we examined the effects of chemogenetic activation of dmPAG^{Tac2} neurons on fighting behaviors. First, we established the baseline level of aggression by administering *Tac2*-Cre mice with normal saline for 30 minutes and subjected them to RI. Forty-eight hours later, these mice were administered with CNO (0.5 mg/kg, i.p.) for 30 minutes and subjected to the RI again (**Figure 5E**). Upon saline administration, *Tac2*^{mCherry} mice had no changes in fighting behaviors, similar to the results of *Tac2*^{mCherry} mice upon chemogenetic inhibition (**Figure 4L-N**). However, following CNO administration, *Tac2*^{hM3Dq} mice exhibited a significantly elevated levels of aggression towards the intruder (**Figure 5F-I**). There was a 3-fold increase in percentage of mice exhibiting fighting behaviors following activation of dmPAG^{Tac2} neurons (**Figure S6D**). In addition, we tested the possible effects of CNO administration on other behavioral performances and failed to observe any obvious effects of chemogenetic activation of dmPAG^{Tac2} neuron in altering locomotion (**Figure S8A-D**) and anxiety-like behaviors (**Figure S8E-H**). In summary, activation of dmPAG^{Tac2} neurons elicits fighting behaviors and increases aggression in male mice without producing obvious effects in the other behaviors tested.

Fighting behaviors alters transcriptional profiles in dmPAG^{Tac2} neurons

The above data demonstrate that the dmPAG^{Tac2} neurons not only are involved, but also play a causal role in fighting behaviors measured by the RI. We next sought to reveal the molecular programs in dmPAG^{Tac2} neurons that altered by fighting behaviors. To this end, we performed TRAP by injecting Cre-dependent AAV vector with eGFP-tagged ribosome protein L10 (**Figure 6A-B**) in the dmPAG of *Tac2*-cre mice. These mice were subjected to the RI or were maintained as home-cage controls (**Figure 6C**, see *Methods*). Sixty minutes after the RI, brain tissues containing dmPAG were collected. Ribosome-associated mRNAs specific to dmPAG^{Tac2} neurons were purified and RNA-sequencing (RNA-seq) were performed. By comparing gene expression between the two groups of immunoprecipitated IP samples (RI vs Control), we identified 58 differentially expressed genes (DEGs) induced by fighting, including 34 upregulated DEGs and 23 downregulated DEGs (**Figure 6D**). KEGG analysis showed that, the pathways impacted by fighting behaviors mainly involved inflammation, immunity and infection-related pathways (**Figure 6E-F**). Of note, the estrogen signaling pathway, which has been previously shown in controlling inter-male aggression behaviors in the VMH (Hashikawa et al., 2017), was identified by our analysis, consistent with the previous notion that estrogen can regulate aggression behaviors (Dombret et al., 2020; Jager et al., 2018; Sano et al., 2013).

To identify novel targets related to fighting, we performed enrichment analysis (Zhao et al., 2017) by calculating fold-enrichment (RI-IP/Ctr-IP) and aligned the top candidate genes (**Figure 6G**). Among the most significantly enriched genes, several well-established immediate-early genes, including *Arc*, *Egr1*, *Fgf2*, and *Fosb*, were upregulated, suggesting that, indeed, the dmPAG^{Tac2} neurons were activated by fighting behaviors and that the TRAP-seq approach was accurate in capturing these molecular events. In downregulated genes, we noticed that *Tph2*, a gene encoding tryptophan hydroxylase 2, a rate-limiting enzyme that is primarily expressed in the serotonergic neurons of the brain, consistent with previously established knowledge that the serotonergic system is involved in aggression at both ligand and receptor levels (Coccaro et al., 2015; Olivier and Mos, 1992; Olivier and van Oorschot, 2005; Vazquez-Leon et al., 2023).

Pharmacological manipulation of dmPAG^{Tac2} neurons in fighting behaviors

To validate the potential molecular pathways in dmPAG^{Tac2} neuron altered by fighting, we targeted 5-HT system identified by TRAP-seq. We hypothesize that intervening 5-HT reuptake thereby increasing 5-HT levels in the extracellular synaptic cleft, as previously demonstrated (Bianchi et al., 2002; Malagie

et al., 1995), could be a means to block the behavioral effects induced by chemogenetic activation of dmPAG^{Tac2} neurons. To this end, we intracranially delivered fluoxetine, a widely used selected 5-HT reuptake inhibitor, into the dmPAG prior to chemogenetic activation (see *Methods*, **Figure 7A**). As expected, in Tac2^{hM3Dq} mice, CNO administration effectively elicited fighting while intra-dmPAG delivery of fluoxetine prevented the chemogenetic activation-elicited fighting behaviors, as showed by a significantly increased latency to attack (**Figure 7B**), decreased number (**Figure 7C)** and duration of attacks (**Figure 7D**), suggesting that targeting 5-HT reuptake in dmPAG neurons could prevent the fighting behaviors elicited by activation of dmPAG^{Tac2} neurons. The above data suggest potential involvement of 5-HT system in dmPAG^{Tac2} neurons-mediated fighting behaviors. We also analyzed the TRAP-seq data mainly focused on 5-HT system-associated genes, including genes that encode 5-HT receptors (**Figure S9)**. The analysis shows RI indeed upregulated gene expression of 5-HT receptors (**Figure S9**).

DISCUSSION

dmPAG^{Tac2} neurons exhibit distinct expression pattern

Tac2^{+} neurons showed a unique distribution pattern in brain of mouse. In the basal level, *Tac2* genes are expressed in a wide variety of brain areas associated with mood and social behaviors, including the BNST, medial habenular (MH), central amygdala (CeA) (Zelikowsky et al., 2018). In pathological states such as prolonged social isolation, Tac2 can be strongly induced to act on the whole brain in a dissociable and region-specific manner (Zelikowsky et al., 2018). The induction pattern of Tac2 peptide or distributed expression of Tac2^{+} neurons suggest that the regulatory roles of the Tac2/NkB signaling in multiple brain functions depend on its anatomical location and neural connection. *Tac2*-expressing neurons located in the dorsomedial shell of the nucleus accumbens is previously characterized as a subtype of D1 medium spiny neurons to play a negative regulatory role in cocaine addiction (Zhao et al., 2022). In CeA, *Tac2*-expressing neurons mainly modulate consolidation of fear memory (Andero et al., 2014; Florido et al., 2021). A recent study showed that *Tac2*-expressing neurons in the BNST and the CeA regulate behavioral states, i.e., emotional valence, by sending inhibitory inputs to the LHA neurons expressing melanin-concentrating hormone (Fujita et al., 2021). These studies suggest that *Tac2*-expressing neurons are uniquely positioned in specific brain regions to modulate behavioral homeostasis.

However, the distribution pattern of Tac2 in the midbrain and the specific functions of Tac2 neurons in corresponding brain regions are not yet clear. In this study, we focus on *Tac2*-expressing neurons of midbrain. Using reporter mice, we revealed that Tac2^{+} neurons were specifically distributed in the PAG especially it's dorsomedial part (dmPAG). The PAG has been traditionally viewed as an integrating center for defensive responses, including panic, fight-flight and freezing behaviors (Deng et al., 2016; Motta et al., 2017). Early studies used c-Fos expression and observed that there was an anatomic segregation of defensive behaviors in the dorsal columns of the PAG (Vianna et al., 2003) and that the dmPAG is served as a relay station for acquiring aversive information to the other brain regions (Borelli et al., 2006). However, it is not clear which cell type mainly mediates this effect. Here, we uncovered that *Tac2*-expressing neurons in the dmPAG (dmPAG^{Tac2} neurons) are key neural substrates that play a critical role in intermale aggression.

dmPAG^{Tac2} neurons are recruited during intermale aggression

Confirming that *Tac2*-expressing neurons in the PAG are mainly located in the dmPAG, we hypothesize that dmPAG^{Tac2} neurons are involved in aggression behaviors. Using a RI paradigm, indeed, we found that fighting behaviors specifically activate dmPAG^{Tac2} neurons, which are shown by induction of c-Fos

and time-locked Ca^{2+} transient examined by fiber photometry (**Figure 3**). These data suggest that dmPAG^{Tac2} neurons are recruited during aggression.

In clinical assessment, aggression behavior can be predominantly categorized into two major subtypes, impulsive aggression or premeditated aggression (Stanford et al., 2003), whereas in animal studies, no consensus has been made in categorizing aggressive behaviors (Fraser and Rushen, 1987). In rodents, several detailed descriptions of fighting types during aggression and defensive behaviors have been suggested in rodents, including play fighting, offensive aggression, defensive aggression, predatory aggression (Blanchard et al., 2003). These terms are intermingled in interpretation of behavioral tasks and might create confusion. One of the limitations of our study is, we mainly assess the role of dmPAG^{Tac2} neurons in intermale aggression, but not in other subtypes of aggressive behaviors such as maternal aggression, when a female defends the newborn pups (Miczek et al., 2001). The PAG is also known as a center in regulating predatory aggression (Zhao et al., 2023), in which the lPAG mainly recruited for sensory processing (Yu et al., 2021) and the vlPAG glutamatergic neurons recruited for conditioned freezing responses (Tovote et al., 2016). However, whether dmPAG^{Tac2} neurons are directly or indirectly involved in predatory aggression is currently unknown and will be an interesting research topic for future study.

Bidirectional manipulation of dmPAG^{Tac2} neuronal activity alters fighting behaviors

We observed that, in the EPM test, *Tac2*-Cre mice spent a modest but significant increased time in the open arms (**Figure S5J**), an index represents anxiolytic-like behavior, similar to a previous report showing that prolonged social isolation causes anxiolytic-like behavior (Zelikowsky et al., 2018). In our chemogenetic experiments, we similarly observed that CNO-induced inhibition of dmPAG^{Tac2} neuronal activity, resembling temporary loss of function of these cells, increased time spent in the open arms (**Figure S7F**). All these data collectively suggest that the Tac2/NkB signaling might be a potential target for anxiety treatment, however, more studies are needed to examine this hypothesis.

Our targeted inhibition and genetic ablation of dmPAG^{Tac2} neuronal activity yielded qualitatively similar results in RI (**Figure 4**), showed by prolonged the latency to attack and significantly reduced numbers and duration of attacks, suggesting suppressed fighting behaviors. Thus, dmPAG^{Tac2} neurons are necessary to mediate fighting behaviors. On the other hand, targeted chemogenetic activation of dmPAG^{Tac2} neuronal activity, however, not only shortened the latency to attack, but also significantly increased numbers and duration of attacks (**Figure 5**), demonstrating that activation of dmPAG^{Tac2} neurons is sufficient to induce fighting behaviors. These striking evidence show that dmPAG^{Tac2} neurons play a critical role in fighting behaviors in male mice. In our chemogenetic manipulation experiment, we chose a controlled before-after study design, therefore to maximally measure the effect of various interventions on the same subjects, providing a better evaluation of variables at baseline and after interventions (Carey et al., 2012). The limitation of this design, however, is that the testing mice would be repeatedly exposed to an intruder mouse, which might cause sensitization to the stimuli. In fact, in clinics, people with high-level of violence and aggression would be very likely to exhibit high frequency of violent behaviors, i.e., physical attacks and verbal aggression towards multiple subjects (Caruso et al., 2021; Schablon et al., 2018). It would be intriguing, in the future, to investigate how transition from acute to repeated exposure of intruders alters dmPAG^{Tac2} neurons activity. Together, these data suggest that dmPAG^{Tac2} neurons regulate fighting behaviors in male mice while without affecting basic behavioral performance.

Role of 5-HT systems in dmPAG^{Tac2} neurons during aggression

The relationship between 5-HT system and aggression has always been an important topic. Male mice

with mutation in gene for monoamine oxidase A exhibited enhanced aggression, accompanied with altered amounts of brain 5-HT levels (Brunner et al., 1993; Cases et al., 1995). Likewise, mice lacking 5-HT_{1B} receptor exhibited intense fighting behaviors towards an intruder (Saudou et al., 1994). Mice with global nNOS KO exhibited high level of aggression related with impaired 5-HT turnover and deficient 5-HT receptor function (Chiavegatto et al., 2001). In our study, potential involvement of 5-HT system in $dmPAG^{Tac2}$ neurons-mediated fighting behaviors has also been found.

Using TRAP-seq, instead of studying the Tac2/NkB signaling or Tac2 peptide, we investigated the translational alteration of *Tac2*-expressing neurons in the dmPAG following RI exposure in mice that were screened for their aggressiveness. we targeted 5-HT system and found inhibition of 5-HT reuptake with fluoxetine can suppress fighting behaviors elicited by activating $dmPAG^{Tac2}$ neurons. These results not only provide a validation to our targets revealed with TRAP-seq, but also confirm with earlier reports showing that 5-HT are indeed key players in intermale aggression (Brunner et al., 1993; Cases et al., 1995; Chiavegatto et al., 2001; Nelson et al., 1995; Saudou et al., 1994).

Potential treatment for humans with exaggerated aggression

Uncontrolled aggression in humans has become a significant threat to the society, not only brings immediate physical harm but also causes chronic stress and pressure that might negatively affect one's mental health (Anderson and Bushman, 2002). In extreme cases, human aggression can evolve into incidents such as homicide or massive shooting (Fields, 2019). Thus, treating subjects to effectively control aggression behaviors are of high importance. In this study, we not only identify a molecularly distinct neuronal cell type in the midbrain that controls intermale aggression, but also uncover several druggable targets that could modulate exaggerated aggressive behaviors.

REFERENCES

Andero, R., Dias, B.G., Ressler, K.J., 2014. A role for Tac2, NkB, and Nk3 receptor in normal and dysregulated fear memory consolidation. Neuron 83, 444-454.

Anderson, C.A., Bushman, B.J., 2002. Human aggression. Annu Rev Psychol 53, 27-51.

Artur de la Villarmois, E., Gabach, L.A., Bianconi, S., Poretti, M.B., Occhieppo, V., Schioth, H.B., Carlini, V.P., Perez, M.F., 2020. Pharmacological NOS-1 Inhibition Within the Hippocampus Prevented Expression of Cocaine Sensitization: Correlation with Reduced Synaptic Transmission. Mol Neurobiol 57, 450-460.

Bianchi, M., Moser, C., Lazzarini, C., Vecchiato, E., Crespi, F., 2002. Forced swimming test and fluoxetine treatment: in vivo evidence that peripheral 5-HT in rat platelet-rich plasma mirrors cerebral extracellular 5-HT levels, whilst 5-HT in isolated platelets mirrors neuronal 5-HT changes. Exp Brain Res 143, 191-197.

Blanchard, R.J., Wall, P.M., Blanchard, D.C., 2003. Problems in the study of rodent aggression. Horm Behav 44, 161-170.

Borelli, K.G., Ferreira-Netto, C., Brandao, M.L., 2006. Distribution of Fos immunoreactivity in the rat brain after freezing or escape elicited by inhibition of glutamic acid decarboxylase or antagonism of GABA-A receptors in the inferior colliculus. Behav Brain Res 170, 84-93.

Brunner, H.G., Nelen, M., Breakefield, X.O., Ropers, H.H., van Oost, B.A., 1993. Abnormal behavior associated with a point mutation in the structural gene for monoamine oxidase A. Science 262, 578-580.

Canteras, N.S., Goto, M., 1999. Fos-like immunoreactivity in the periaqueductal gray of rats exposed to a natural predator. Neuroreport 10, 413-418.

Carey, T.S., Sanders, G.D., Viswanathan, M., Trikalinos, T.A., Kato, E., Chang, S., 2012. Framework for Considering Study Designs for Future Research Needs, Rockville (MD).

Carlini, V.P., Gaydou, R.C., Schioth, H.B., de Barioglio, S.R., 2007. Selective serotonin reuptake inhibitor (fluoxetine) decreases the effects of ghrelin on memory retention and food intake. Regul Pept 140, 65-73.

Carreno Gutierrez, H., O'Leary, A., Freudenberg, F., Fedele, G., Wilkinson, R., Markham, E., van Eeden, F., Reif, A., Norton, W.H.J., 2020. Nitric oxide interacts with monoamine oxidase to modulate aggression and anxiety-like behaviour. Eur Neuropsychopharmacol 30, 30-43.

Carrive, P., 1993. The periaqueductal gray and defensive behavior: functional representation and neuronal organization. Behav Brain Res 58, 27-47.

Caruso, R., Antenora, F., Riba, M., Belvederi Murri, M., Biancosino, B., Zerbinati, L., Grassi, L., 2021. Aggressive Behavior and Psychiatric Inpatients: a Narrative Review of the Literature with a Focus on the European Experience. Curr Psychiatry Rep 23, 29.

Cases, O., Seif, I., Grimsby, J., Gaspar, P., Chen, K., Pournin, S., Muller, U., Aguet, M., Babinet, C., Shih, J.C., et al., 1995. Aggressive behavior and altered amounts of brain serotonin and norepinephrine in mice lacking MAOA. Science 268, 1763-1766.

Chen, A.X., Yan, J.J., Zhang, W., Wang, L., Yu, Z.X., Ding, X.J., Wang, D.Y., Zhang, M., Zhang, Y.L., Song, N., Jiao, Z.L., Xu, C., Zhu, S.J., Xu, X.H., 2020. Specific Hypothalamic Neurons Required for Sensing Conspecific Male Cues Relevant to Inter-male Aggression. Neuron 108, 763-774 e766.

Chen, Z., Chen, X., Liu, M., Liu, S., Yu, S., Ma, L., 2018. Magnetic Resonance Image Texture Analysis of the Periaqueductal Gray Matter in Episodic Migraine Patients without T2-Visible Lesions. Korean J Radiol 19, 85-92.

Chiavegatto, S., Dawson, V.L., Mamounas, L.A., Koliatsos, V.E., Dawson, T.M., Nelson, R.J., 2001. Brain serotonin dysfunction accounts for aggression in male mice lacking neuronal nitric oxide synthase. Proc Natl Acad Sci U S A 98, 1277-1281.

Coccaro, E.F., Fanning, J.R., Phan, K.L., Lee, R., 2015. Serotonin and impulsive aggression. CNS Spectr 20, 295-302.

Deng, H., Xiao, X., Wang, Z., 2016. Periaqueductal Gray Neuronal Activities Underlie Different Aspects of Defensive Behaviors. J Neurosci 36, 7580-7588.
Dielenberg, R.A., Hunt, G.E., McGregor, I.S., 2001. "When a rat smells a cat": the distribution of Fos immunoreactivity in rat brain following exposure to a predatory odor. Neuroscience 104, 1085-1097.
Dombret, C., Naule, L., Trouillet, A.C., Parmentier, C., Hardin-Pouzet, H., Mhaouty-Kodja, S., 2020. Effects of neural estrogen receptor beta deletion on social and mood-related behaviors and underlying mechanisms in male mice. Sci Rep 10, 6242.
Falkner, A.L., Wei, D., Song, A., Watsek, L.W., Chen, I., Chen, P., Feng, J.E., Lin, D., 2020. Hierarchical Representations of Aggression in a Hypothalamic-Midbrain Circuit. Neuron 106, 637-648 e636.
Fields, R.D., 2019. THE ROOTS OF HUMAN AGGRESSION: Experiments in humans and animals have started to identify how violent behaviors begin in the brain. Sci Am 320, 65-71.
Florido, A., Velasco, E.R., Soto-Faguas, C.M., Gomez-Gomez, A., Perez-Caballero, L., Molina, P., Nadal, R., Pozo, O.J., Saura, C.A., Andero, R., 2021. Sex differences in fear memory consolidation via Tac2 signaling in mice. Nat Commun 12, 2496.
Franklin, T.B., 2019. Recent Advancements Surrounding the Role of the Periaqueductal Gray in Predators and Prey. Front Behav Neurosci 13, 60.
Fraser, D., Rushen, J., 1987. Aggressive behavior. Vet Clin North Am Food Anim Pract 3, 285-305.
Fujita, A., Zhong, L., Antony, M.S., Chamiec-Case, E., Mickelsen, L.E., Kanoski, S.E., Flynn, W.F., Jackson, A.C., 2021. Neurokinin B-Expressing Neurons of the Central Extended Amygdala Mediate Inhibitory Synaptic Input onto Melanin-Concentrating Hormone Neuron Subpopulations. J Neurosci 41, 9539-9560.
Hashikawa, K., Hashikawa, Y., Tremblay, R., Zhang, J., Feng, J.E., Sabol, A., Piper, W.T., Lee, H., Rudy, B., Lin, D., 2017. Esr1(+) cells in the ventromedial hypothalamus control female aggression. Nat Neurosci 20, 1580-1590.
Heiman, M., Kulicke, R., Fenster, R.J., Greengard, P., Heintz, N., 2014. Cell type-specific mRNA purification by translating ribosome affinity purification (TRAP). Nat Protoc 9, 1282-1291.
Hunsperger, R.W., 1956. [Affective reaction from electric stimulation of brain stem in cats]. Helv Physiol Pharmacol Acta 14, 70-92.
Hunsperger, R.W., Bucher, V.M., 1967. Affective behaviour by electrical stimulation in the forebain and brain stem of the cat. Prog Brain Res 27, 103-127.
Jager, A., Maas, D.A., Fricke, K., de Vries, R.B., Poelmans, G., Glennon, J.C., 2018. Aggressive behavior in transgenic animal models: A systematic review. Neurosci Biobehav Rev 91, 198-217.
Karigo, T., Kennedy, A., Yang, B., Liu, M., Tai, D., Wahle, I.A., Anderson, D.J., 2021. Distinct hypothalamic control of same- and opposite-sex mounting behaviour in mice. Nature 589, 258-263.
Koolhaas, J.M., Coppens, C.M., de Boer, S.F., Buwalda, B., Meerlo, P., Timmermans, P.J., 2013. The resident-intruder paradigm: a standardized test for aggression, violence and social stress. J Vis Exp, e4367.
Kretschmer, T., Ouellet-Morin, I., Vrijen, C., Nolte, I.M., Hartman, C., 2023. Polygenic risk for aggressive behavior from late childhood through early adulthood. Eur Child Adolesc Psychiatry 32, 651-660.
Lee, E.H., Lin, W.R., Chen, H.Y., Shiu, W.H., Liang, K.C., 1992. Fluoxetine and 8-OH-DPAT in the lateral septum enhances and impairs retention of an inhibitory avoidance response in rats. Physiol Behav 51, 681-688.
Li, Y.J., Li, C.Y., Li, C.Y., Hu, D.X., Xv, Z.B., Zhang, S.H., Li, Q., Zhang, P., Tian, B., Lan, X.L., Chen, X.Q., 2023. KMT2E Haploinsufficiency Manifests Autism-Like Behaviors and Amygdala Neuronal Development Dysfunction in Mice. Mol Neurobiol 60, 1609-1625.
Linnman, C., Moulton, E.A., Barmettler, G., Becerra, L., Borsook, D., 2012. Neuroimaging of the periaqueductal gray: state of the field. Neuroimage 60, 505-522.
Lischinsky, J.E., Lin, D., 2020. Neural mechanisms of aggression across species. Nat Neurosci 23,

1317-1328.
MacLaren, D.A., Browne, R.W., Shaw, J.K., Krishnan Radhakrishnan, S., Khare, P., Espana, R.A., Clark, S.D., 2016. Clozapine N-Oxide Administration Produces Behavioral Effects in Long-Evans Rats: Implications for Designing DREADD Experiments. eNeuro 3.
Malagie, I., Trillat, A.C., Jacquot, C., Gardier, A.M., 1995. Effects of acute fluoxetine on extracellular serotonin levels in the raphe: an in vivo microdialysis study. Eur J Pharmacol 286, 213-217.
Mar, L., Yang, F.C., Ma, Q., 2012. Genetic marking and characterization of Tac2-expressing neurons in the central and peripheral nervous system. Mol Brain 5, 3.
Miczek, K.A., Maxson, S.C., Fish, E.W., Faccidomo, S., 2001. Aggressive behavioral phenotypes in mice. Behav Brain Res 125, 167-181.
Motta, S.C., Carobrez, A.P., Canteras, N.S., 2017. The periaqueductal gray and primal emotional processing critical to influence complex defensive responses, fear learning and reward seeking. Neurosci Biobehav Rev 76, 39-47.
Nelson, R.J., Demas, G.E., Huang, P.L., Fishman, M.C., Dawson, V.L., Dawson, T.M., Snyder, S.H., 1995. Behavioural abnormalities in male mice lacking neuronal nitric oxide synthase. Nature 378, 383-386.
Olivier, B., Mos, J., 1992. Rodent models of aggressive behavior and serotonergic drugs. Prog Neuropsychopharmacol Biol Psychiatry 16, 847-870.
Olivier, B., van Oorschot, R., 2005. 5-HT1B receptors and aggression: a review. Eur J Pharmacol 526, 207-217.
Ota, K.T., Monsey, M.S., Wu, M.S., Schafe, G.E., 2010. Synaptic plasticity and NO-cGMP-PKG signaling regulate pre- and postsynaptic alterations at rat lateral amygdala synapses following fear conditioning. PLoS One 5, e11236.
Park, S.G., Jeong, Y.C., Kim, D.G., Lee, M.H., Shin, A., Park, G., Ryoo, J., Hong, J., Bae, S., Kim, C.H., Lee, P.S., Kim, D., 2018. Medial preoptic circuit induces hunting-like actions to target objects and prey. Nat Neurosci 21, 364-372.
Qi, G., Zhang, P., Li, T., Li, M., Zhang, Q., He, F., Zhang, L., Cai, H., Lv, X., Qiao, H., Chen, X., Ming, J., Tian, B., 2022. NAc-VTA circuit underlies emotional stress-induced anxiety-like behavior in the three-chamber vicarious social defeat stress mouse model. Nat Commun 13, 577.
Sano, K., Tsuda, M.C., Musatov, S., Sakamoto, T., Ogawa, S., 2013. Differential effects of site-specific knockdown of estrogen receptor alpha in the medial amygdala, medial pre-optic area, and ventromedial nucleus of the hypothalamus on sexual and aggressive behavior of male mice. Eur J Neurosci 37, 1308-1319.
Saudou, F., Amara, D.A., Dierich, A., LeMeur, M., Ramboz, S., Segu, L., Buhot, M.C., Hen, R., 1994. Enhanced aggressive behavior in mice lacking 5-HT1B receptor. Science 265, 1875-1878.
Schablon, A., Wendeler, D., Kozak, A., Nienhaus, A., Steinke, S., 2018. Prevalence and Consequences of Aggression and Violence towards Nursing and Care Staff in Germany-A Survey. Int J Environ Res Public Health 15.
Schreiner, L., Kling, A., 1953. Behavioral changes following rhinencephalic injury in cat. J Neurophysiol 16, 643-659.
Shen, F., Wang, N., Qi, C., Li, Y.J., Cui, C.L., 2014. The NO/sGC/PKG signaling pathway in the NAc shell is necessary for the acquisition of morphine-induced place preference. Behav Neurosci 128, 446-459.
Silva, C., McNaughton, N., 2019. Are periaqueductal gray and dorsal raphe the foundation of appetitive and aversive control? A comprehensive review. Prog Neurobiol 177, 33-72.
Stanford, M.S., Houston, R.J., Mathias, C.W., Villemarette-Pittman, N.R., Helfritz, L.E., Conklin, S.M., 2003. Characterizing aggressive behavior. Assessment 10, 183-190.
Takeda, I., Yoshihara, K., Cheung, D.L., Kobayashi, T., Agetsuma, M., Tsuda, M., Eto, K., Koizumi, S., Wake, H., Moorhouse, A.J., Nabekura, J., 2022. Controlled activation of cortical astrocytes modulates neuropathic pain-like behaviour. Nat Commun 13, 4100.

Tecott, L.H., Barondes, S.H., 1996. Genes and aggressiveness. Behavioral genetics. Curr Biol 6, 238-240.
Tovote, P., Esposito, M.S., Botta, P., Chaudun, F., Fadok, J.P., Markovic, M., Wolff, S.B., Ramakrishnan, C., Fenno, L., Deisseroth, K., Herry, C., Arber, S., Luthi, A., 2016. Midbrain circuits for defensive behaviour. Nature 534, 206-212.
Vazquez-Leon, P., Miranda-Paez, A., Valencia-Flores, K., Sanchez-Castillo, H., 2023. Defensive and Emotional Behavior Modulation by Serotonin in the Periaqueductal Gray. Cell Mol Neurobiol 43, 1453-1468.
Vianna, D.M., Borelli, K.G., Ferreira-Netto, C., Macedo, C.E., Brandao, M.L., 2003. Fos-like immunoreactive neurons following electrical stimulation of the dorsal periaqueductal gray at freezing and escape thresholds. Brain Res Bull 62, 179-189.
Wall, N.R., Wickersham, I.R., Cetin, A., De La Parra, M., Callaway, E.M., 2010. Monosynaptic circuit tracing in vivo through Cre-dependent targeting and complementation of modified rabies virus. Proc Natl Acad Sci U S A 107, 21848-21853.
Xu, Y., Lu, Y., Cassidy, R.M., Mangieri, L.R., Zhu, C., Huang, X., Jiang, Z., Justice, N.J., Xu, Y., Arenkiel, B.R., Tong, Q., 2019. Identification of a neurocircuit underlying regulation of feeding by stress-related emotional responses. Nat Commun 10, 3446.
Yu, H., Xiang, X., Chen, Z., Wang, X., Dai, J., Wang, X., Huang, P., Zhao, Z.D., Shen, W.L., Li, H., 2021. Periaqueductal gray neurons encode the sequential motor program in hunting behavior of mice. Nat Commun 12, 6523.
Zelikowsky, M., Hui, M., Karigo, T., Choe, A., Yang, B., Blanco, M.R., Beadle, K., Gradinaru, V., Deverman, B.E., Anderson, D.J., 2018. The Neuropeptide Tac2 Controls a Distributed Brain State Induced by Chronic Social Isolation Stress. Cell 173, 1265-1279 e1219.
Zha, X., Wang, L., Jiao, Z.L., Yang, R.R., Xu, C., Xu, X.H., 2020. VMHvl-Projecting Vglut1+ Neurons in the Posterior Amygdala Gate Territorial Aggression. Cell Rep 31, 107517.
Zhang, Q., Hu, D.X., He, F., Li, C.Y., Qi, G.J., Cai, H.W., Li, T.X., Ming, J., Zhang, P., Chen, X.Q., Tian, B., 2019. Locus coeruleus-CA1 projections are involved in chronic depressive stress-induced hippocampal vulnerability to transient global ischaemia. Nat Commun 10, 2942.
Zhao, Z.D., Han, X., Chen, R., Liu, Y., Bhattacherjee, A., Chen, W., Zhang, Y., 2022. A molecularly defined D1 medium spiny neuron subtype negatively regulates cocaine addiction. Sci Adv 8, eabn3552.
Zhao, Z.D., Yang, W.Z., Gao, C., Fu, X., Zhang, W., Zhou, Q., Chen, W., Ni, X., Lin, J.K., Yang, J., Xu, X.H., Shen, W.L., 2017. A hypothalamic circuit that controls body temperature. Proc Natl Acad Sci U S A 114, 2042-2047.
Zhao, Z.D., Zhang, L., Xiang, X., Kim, D., Li, H., Cao, P., Shen, W.L., 2023. Neurocircuitry of Predatory Hunting. Neurosci Bull 39, 817-831.
Zhu, Z., Ma, Q., Miao, L., Yang, H., Pan, L., Li, K., Zeng, L.H., Zhang, X., Wu, J., Hao, S., Lin, S., Ma, X., Mai, W., Feng, X., Hao, Y., Sun, L., Duan, S., Yu, Y.Q., 2021. A substantia innominata-midbrain circuit controls a general aggressive response. Neuron 109, 1540-1553 e1549.

Figures and Figure Legends

Figure 1

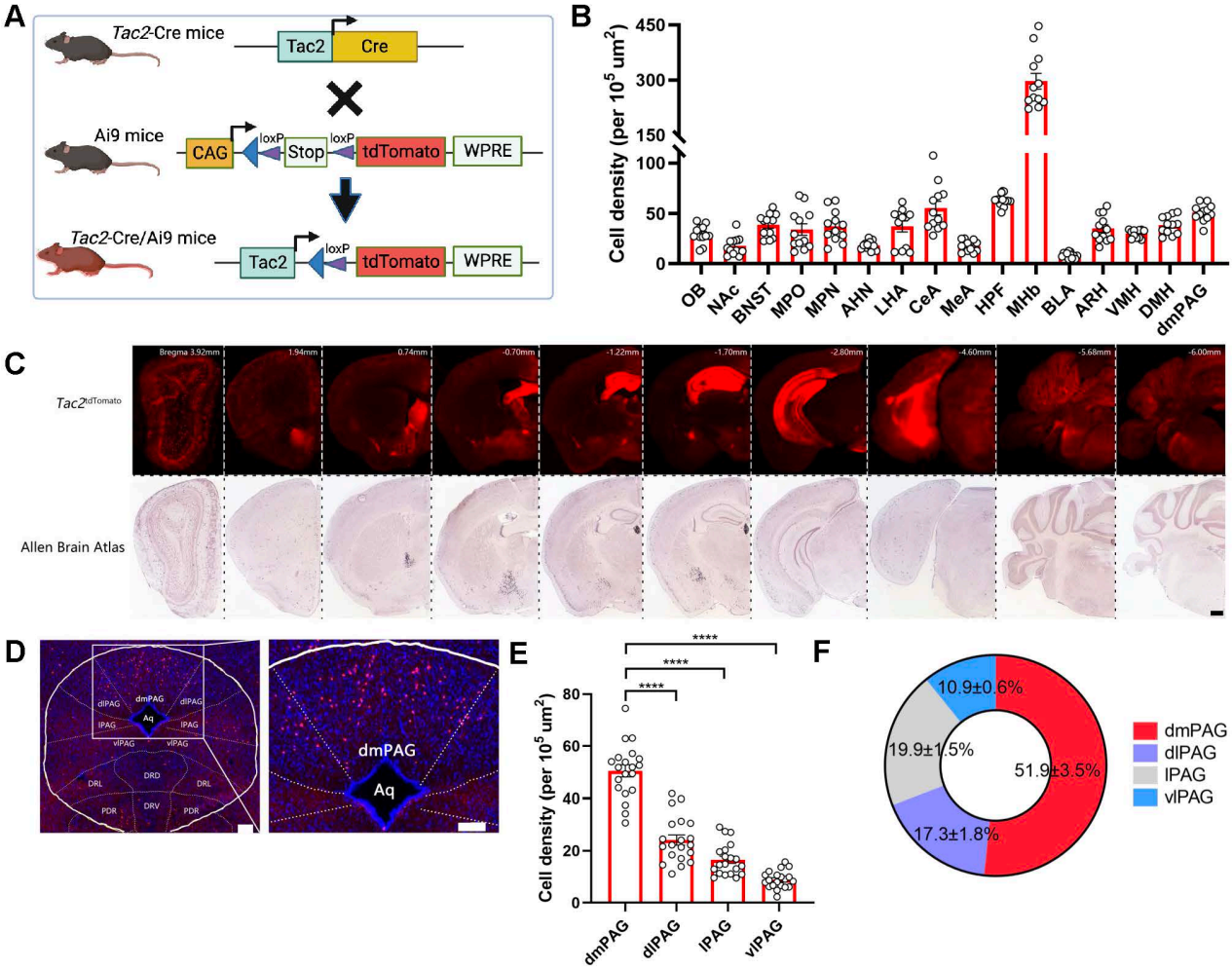

<u>Figure 1</u>. PAG *Tac2*-expressing neurons are mainly located in the dmPAG.

(A) Schematic showing breeding strategy to selectively express tdTomato reporter in Tac2$^+$ cells. (**B**) Whole-brain analysis of Tac2^{tdTomato} cell density. Four series of representative images from N = 3 mice were analyzed. **(C)** Representative fluorescent images showing tdTomato-labeled Tac2$^+$ cells (red) in coronal brain sections in *Tac2*-Cre/Ai9 mice (upper panels) and in their respective ABA images (lower panels). Scale bar, 500 μm. **(D)** Distribution pattern of Tac2$^+$ cells in the PAG subregions. Scale bars, 1,000 μm (left) and 100 μm (right, enlarged view), respectively. **(E)** Analysis of Tac2^{tdTomato} cells in PAG subregions. Four series of representative images from N = 5 mice. **(F)** Pie chart showing percentage of Tac2^{tdTomato} cells in PAG subregions. A total of 648 Tac2$^+$ cells were included from N = 3 mice. Data were expressed as mean ± S.E.M. Significance was calculated by One-way ANOVA and Tukey's multiple comparisons test, **** $P < 0.0001$.

Figure 2

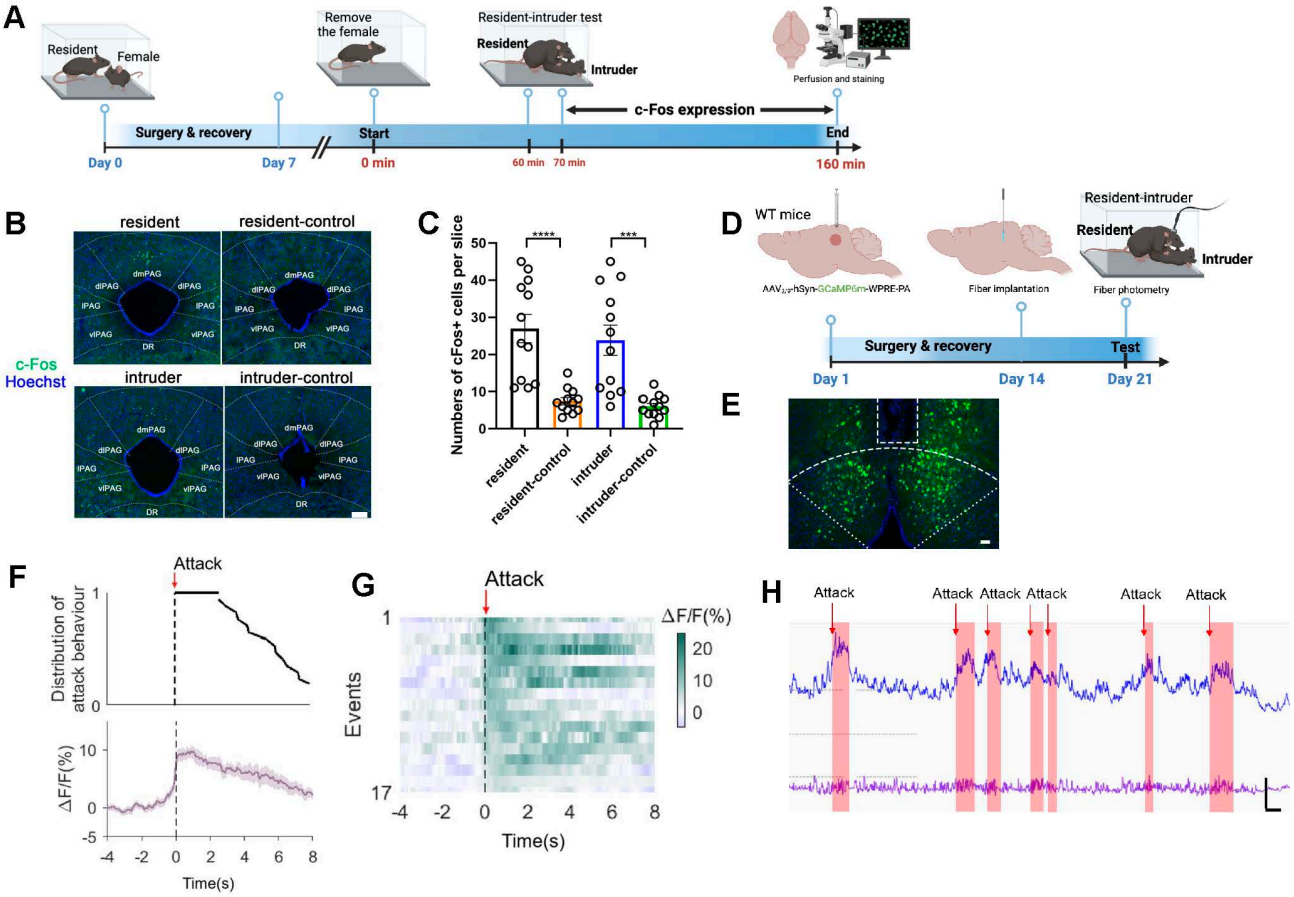

<u>Figure 2</u>. dmPAG neurons respond to aggression

(**A**) Strategy for mapping c-Fos expression in WT mice subjected to the RI test. See ***Methods*** for detailed procedure. (**B**) c-Fos activation in dmPAG of mice from various groups. Scale bar, 100 µm. (**C**) Number of c-Fos^{+} cells in the dmPAG of WT mice. N = 3 mice/group. (**D**) Strategy for *in vivo* fiber photometry in WT mice injected with AAV-hSyn-GCaMP6m. (**E**) Fiber position targeting the dmPAG of WT mice. Scale bar, 50 µm. **(F)** Distribution of attack behavior synchronized with ΔF/F%. (**G**) Heatmap showing Ca^{2+} activity time-locked to an attack episode. x-axis shows 4 sec prior to and 8 sec after the attack episode (red arrow). (**H**) Representative Ca^{2+} trace showing one trial of Ca^{2+} activity in a WT mouse during the RI test. Scale bar: 10s in x-axis and 2000 A.U. in y-axis. Baseline (bottom trace): reference control channel (405 nm); upper trace, Ca^{2+} channel (470 nm). Red shaded areas indicate attack episodes and durations. Data represent mean ± S.E.M. Significance was calculated by One-way ANOVA and Tukey's multiple comparisons test, *** $P < 0.001$, **** $P < 0.0001$.

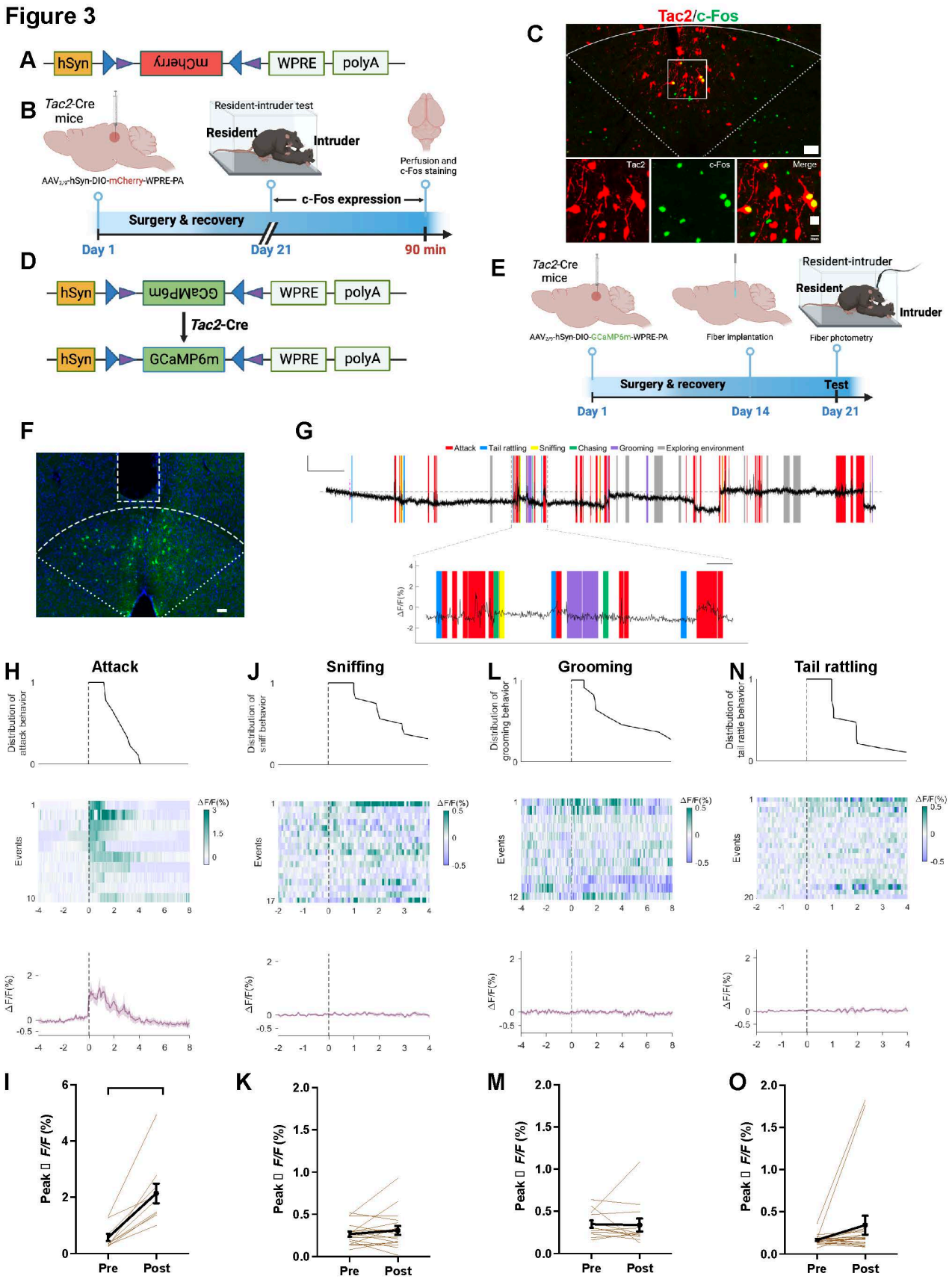

Figure 3. ***Tac2*-expressing neurons in dmPAG respond to aggression**

(A) Vector information for AAV-hSyn-DIO-mCherry. (**B**) Strategy for examining activation of Tac2^{+} neuron by fighting behaviors. AAV vector was injected to *Tac2*-Cre mice to drive mCherry expression in dmPAG^{Tac2} neurons.

See ***Methods*** for detailed procedure. (**C**) c-Fos expression (green) in dmPAG^{Tac2} neurons (red mCherry labeled) in *Tac2*-Cre mice subjected to the RI test. Lower panels showing enlarged view from the white box in the upper panel. Scale bars, 50 μm (upper), 20 μm (lower), respectively. (**D**) Vector information for AAV-hSyn-DIO-GcaMP6m in *Tac2*-Cre mice. (**E**) Strategy for *in vivo* fiber photometry in *Tac2*-Cre mice injected with a Cre-dependent AAV-GcaMP6m vector. (**F**) Fiber position targeting dmPAG region of Tac2 mice. Scale bar, 50 μm. (**G**) Example recording of dmPAG^{Tac2} neurons during the RI test. Color shades indicate different behavioral syllables during intruder encounter. Scale bar: 60s in x-axis, 1.5% GCaMP6m ΔF/F signal in Y-axis. (**H-O**) Ca^{2+} activity time-locked to attack (H-I), sniffing (J-K), grooming (L-M) and tail rattling (N-O). (H) distribution of attack events (top), heatmap of GCaMP6m ΔF/F signals (middle) and ΔF/F% (bottom), (I) analysis of peak ΔF/F before (Pre) and after (Post) each attack episode. The other panels present the same manner but with different behavioral syllables, including sniffing (J-K), grooming (L-M), and tail rattle (N-O). Data represent mean ± S.E.M. Paired *t*-test, ***$P < 0.001$.

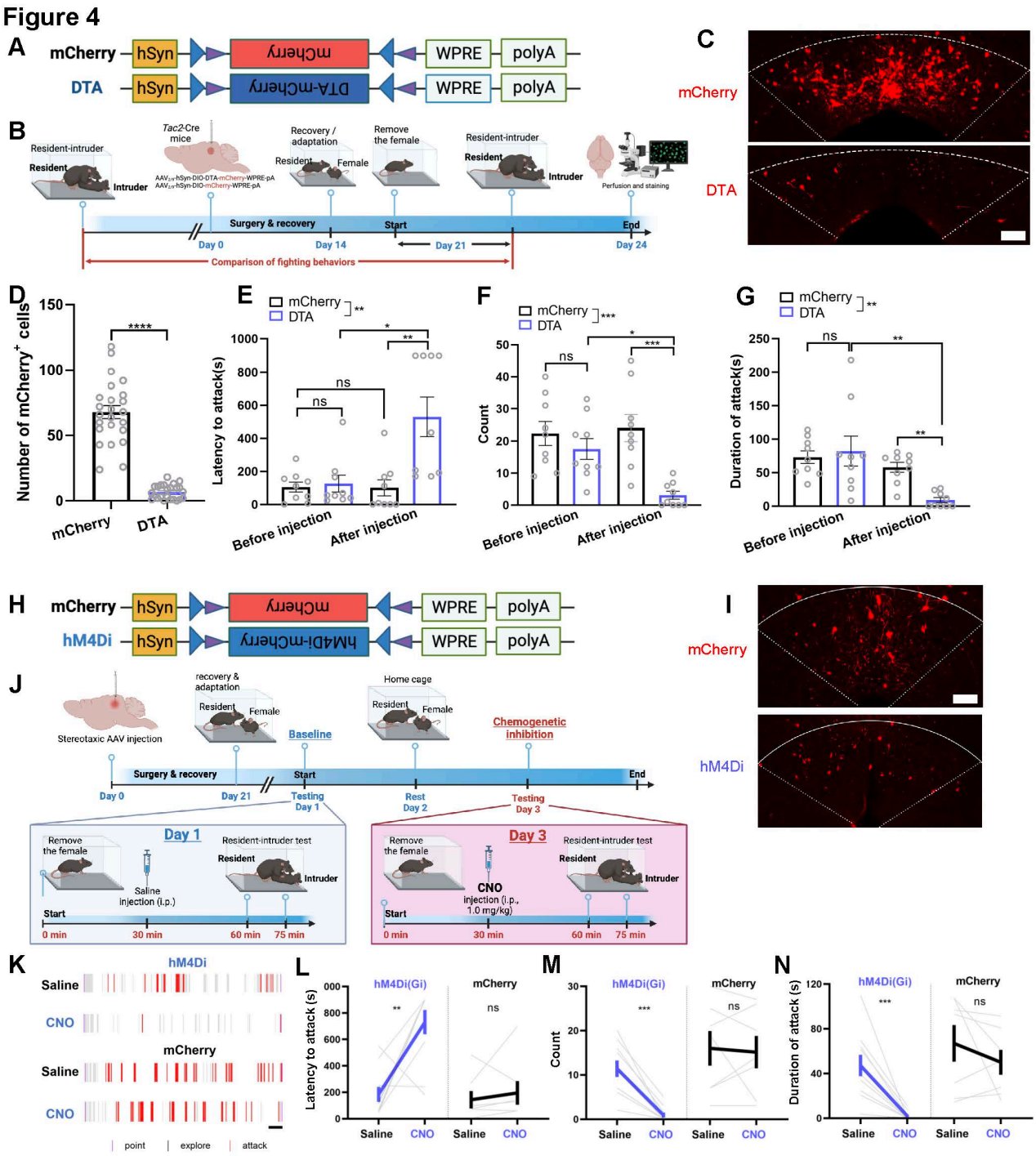

Figure 4. Ablation or inhibition of dmPAG^{Tac2} neurons suppresses fighting behaviors

(A) A Cre-dependent DTA vector or its control vector to be expressed in dmPAG^{Tac2} neurons. **(B)** Strategy for genetic ablation. **(C)** Validation of DTA (bottom) and control AAV (upper) in *Tac2*-cre mouse. Scale bar, 100 μm**.** **(D)** Number of mCherry^{+} cells in dmPAG in *Tac2*-Cre mice receiving genetic ablation. N = 6 mice. **(E-G)** Analysis of latency to attack (E), number of attack (F) and duration of attack (G). N = 9/group. Significance was calculated with Two-way RM ANOVA followed by Tukey's multiple comparisons test. **P* < 0.05, ***P* < 0.01, ****P* < 0.001. (**H**) a Cre-dependent hM4Di vector or its control to be expressed in dmPAG^{Tac2} neurons. **(I)** Representative fluorescent images of mCherry (upper) or hM4Di-mCherry (bottom). Scale bar, 100 μm. **(J)** Strategy for the RI test in *Tac2*-Cre mice receiving inhibitory DREADDs vectors. **(K)** Raster plots showing mouse attack (red bar) or exploring behaviors (gray bar) during the RI assay. Scale, 1 min. (**L-N**) Analysis of latency to attacks (**L**), number of attacks (**M**) and duration of attacks (**N**). N = 10 in *Tac2*^{hM4Di} group and N = 7 in *Tac2*^{mCherry} group. Data represent mean ± S.E.M. Significance was calculated by means of paired *t*-test. ***P* < 0.01, ****P* < 0.001.

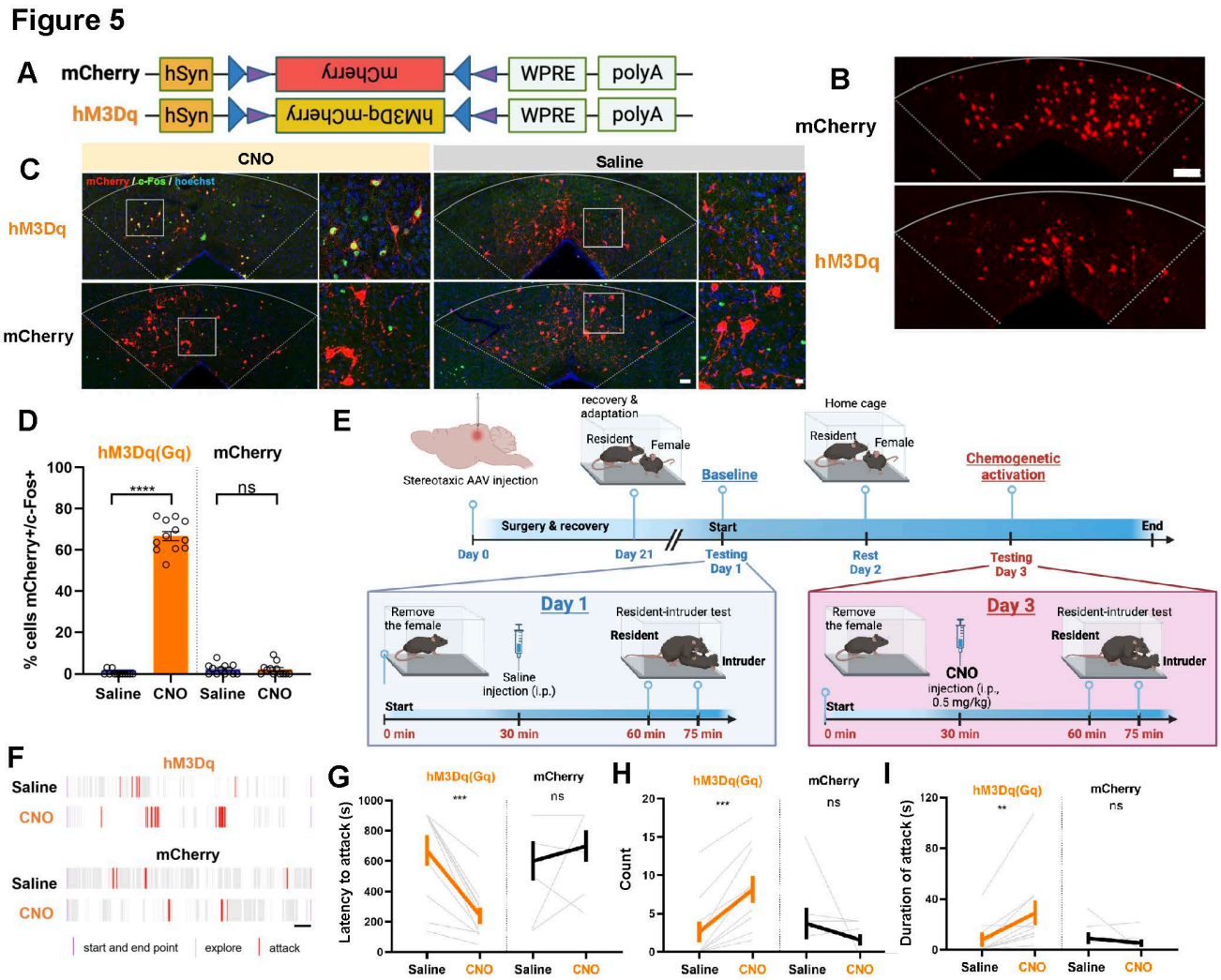

<u>Figure 5</u>. Chemogenetic activation of dmPAG^{Tac2} neurons elicits fighting behaviors.

(A) A Cre-dependent hM3Dq vector or its control vector to be expressed in dmPAG^{Tac2} neurons. **(B)** Representative fluorescent images of hM3Dq-mCherry or mCherry (red) in dmPAG^{Tac2} neurons. Scale bar, 100 μm. **(C)** Double immunofluorescent staining of mCherry and c-Fos (red: mCherry; green: c-Fos; blue: Hoechst). Scale bars, 50 μm (left) and 10 μm (enlarged right panel), respectively. (**D**) Number of mCherry^{+} cells in c-Fos^{+} neurons in *Tac2*-Cre mice receiving CNO injection (0.5 mg/kg, *i.p.*). Four series of representative images from N = 3 mice. (**E**) Strategy for the RI test in *Tac2*-Cre mice receiving DREADDs vectors. (**F**) Raster plots showing mouse attack (red) or exploring behavior (gray) during the RI test. Time scale, 1 min. (**G-I**) Analysis of latency to attack (**G**), number of attack (**H**), and duration of attack (**I**). N = 10 in *Tac2*^{hM3Dq} group and N = 7 in *Tac2*^{mCherry} group. Data represent mean ± S.E.M. Significance was calculated by means of paired *t*-test. $^{**}P < 0.01$, $^{***}P < 0.001$, $^{****}P < 0.0001$.

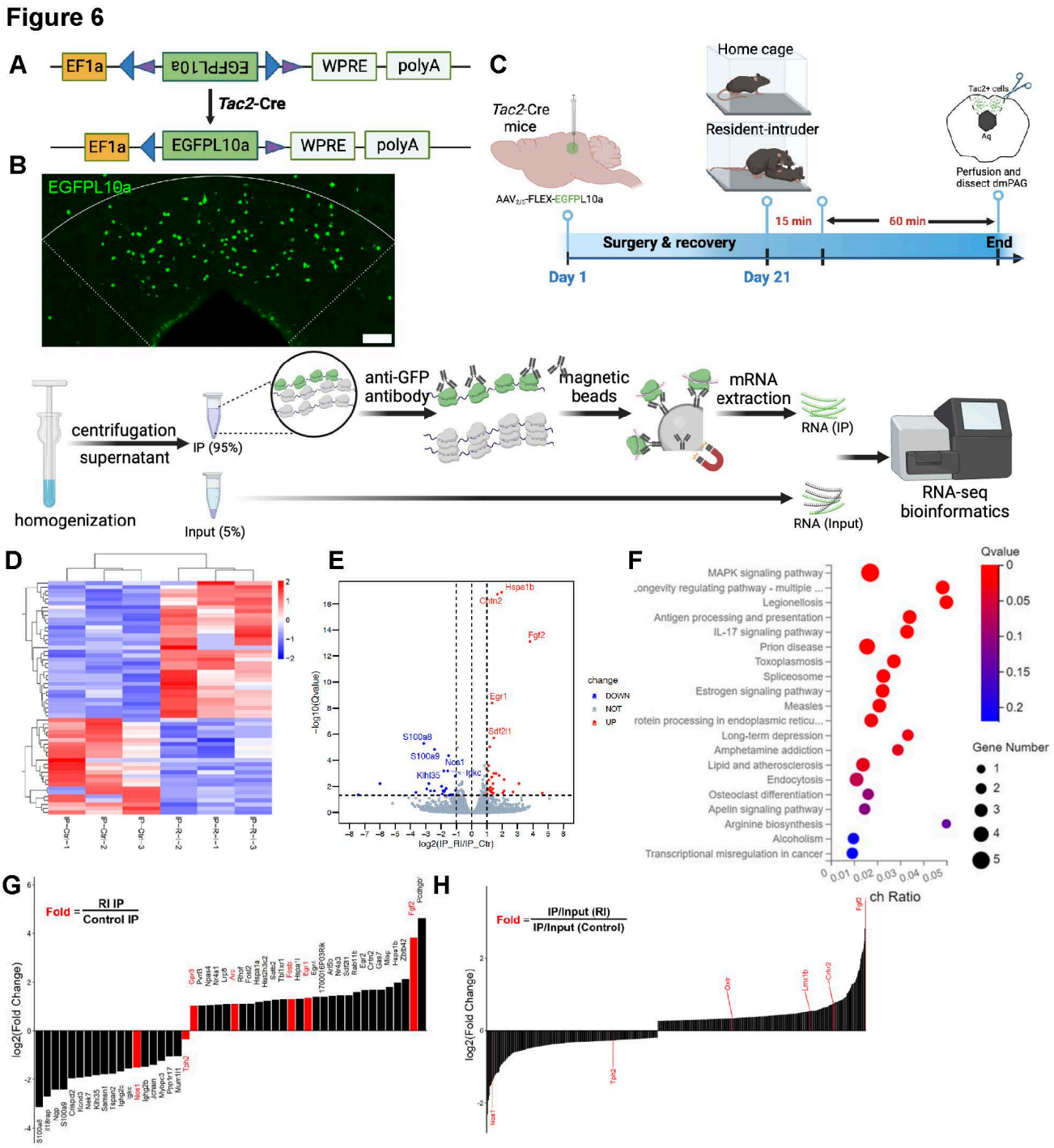

Figure 6. TRAP-seq reveals transcriptional alterations following fighting behaviors

(A) A Cre-dependent TRAP (AAV-FLEX-EGFPL10a) vector to be expressed in *Tac2*-Cre mice. **(B)** Representative fluorescent images of EGFPL10a protein (green) in dmPAG. Scale bar, 100 μm. **(C)** Strategy for TRAP-seq in *Tac2*-Cre mice injected with AAV-FLEX-EGFPL10a in dmPAG and subjected to the RI assay or maintained at home cage (control). **(D)** Heatmap showing DEGs of the IP samples. $|Log_2FC|>1$, adjusted q value < 0.05. **(E)** Volcano plot showing DEGs of the IP samples. **(F)** KEGG enrichment analysis showing top 20 most enriched pathways affected by RI when compared to the control. **(G)** Fold-change analysis showing $log_2(FC)$ value of RI-IP to Control-IP samples. Genes labeled in red are immediate-early genes (*Gpr3*, *Arc*, *Fosb*, *Egr1*, *Fgf2*) or genes enlisted for subsequent validation experiment (*Trph2*). **(H)** A secondary analysis of enrichment score, based on normalizing IR/Input (RI) to IR/Input (Control). Note that *Nos1*, *Tph2*, *Oxtr*, *Lmx1b*, *Crhr2*, and *Fgf2* (labeled in red on the left) were listed among the most enriched genes that were related to the 5-HT system.

Figure 7

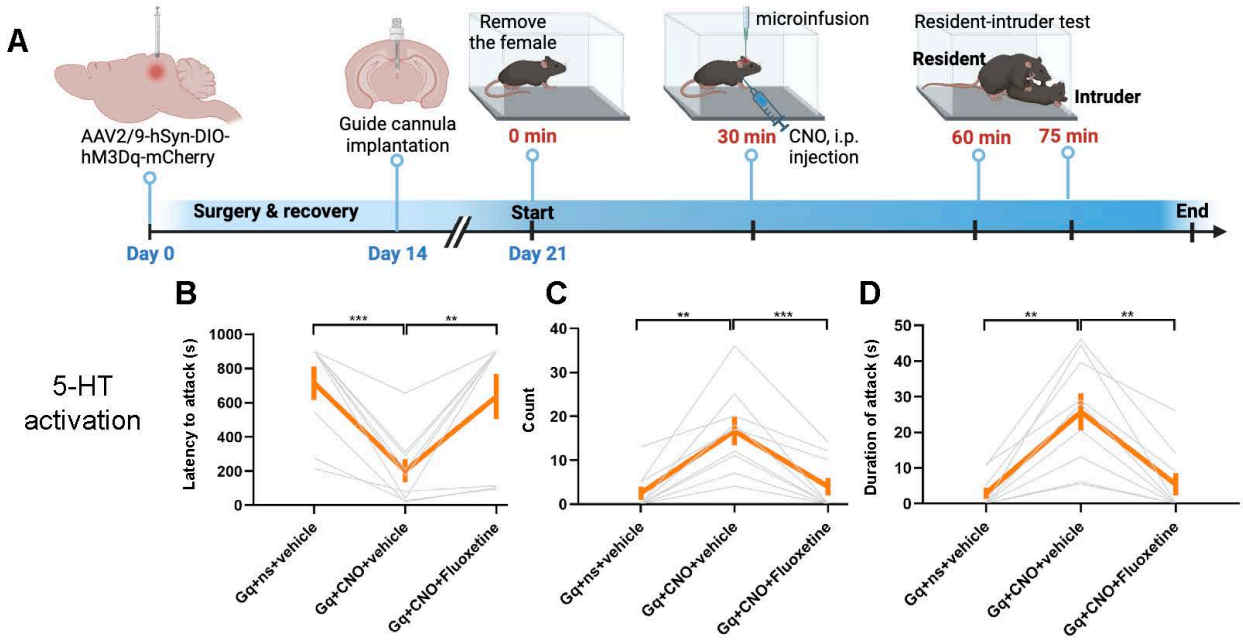

<u>Figure 7</u>. Pharmacological validation of molecular targets identified by TRAP-seq.

(**A)** Strategy for activation of the 5-HT system with fluoxetine microinfusion to suppress fighting behaviors induced by chemogenetic activation of dmPAG^{Tac2} neurons. (**B-D**) Analysis of latency to attack (**B**), number of attack (**C**) and duration of attack (**D**) in Tac2^{hM3dq} mice injected with fluoxetine/vehicle and CNO/saline at dmPAG. N = 9 mice/group. Data represent mean ± SEM. Significance was calculated by means of paired *t*-test. * $P < 0.05$, ** $P < 0.01$, *** $P < 0.001$, **** $P < 0.0001$.

Supplementary Figure Legends

Figure S1. **PAG *Tac2*-expressing neurons are mainly located in the dmPAG** (related to Figure 1).

(A) Representative fluorescent images showing absence of TdTomato-labeled $Tac2^+$ cells in control mice (*Tac2*-Cre, Ai9, or WT C57BL/6 mice). Scale bars, 500 μm. (B) *Tac2* mRNA expression pattern in ABA ISH database (left), with an enlarged view (right) from the left panel. (C) Distribution pattern of $Tac2^+$ cells in PAG subregions examined fluorescence ISH. Scale bars, 50 μm. (D) Pie chart showing numbers of $Tac2^{tdTomato}$ cells in PAG subregions. N = 3 mice. Data were expressed as mean ± S.E.M.

Figure S2. **Mapping of c-Fos expression in WT mice subjected to the RI assay** (related to Figure 2)

(A) Brain areas with high-level c-Fos expression in WT mice subjected to the RI assay. Scale bar, 1,000 μm. **(B)** Representative fluorescent image showing multiple hypothalamic subnuclei were activated by the RI assay, including the PVT, SBPV, PVZ, AHN, LHA, BLA, DMH, VMH, MRN, and PAG. Scale bar, 100 μm. **(C)** Quantification of number of Fos+ cells in selected brain areas in WT mice subjected to the RI assay. Data are presented as total number of Fos+ cells in five brain sections separated by 200 μm (N = 3 mouse per condition). Data were expressed as mean ± S.E.M. *Abbreviations*: PVT, Paraventricular nucleus of the thalamus; SBPV, Subparaventricular zone hypothalamus; PVZ, Periventricular zone; AHN, Anterior hypothalamic nucleus; LHA, Lateral hypothalamic area; BLA, Basolateral amygdala nucleus, DMH, Dorsomedial nucleus of the hypothalamus; VMH, Ventromedial hypothalamic nucleus; MRN, Midbrain reticular nucleus; PAG, Periaqueductal gray.

Figure S3. **Using a Cre-out strategy to test the role of $dmPAG^{Tac2}$ negative neurons in aggression** (related to Figure 3)

(A) Schematic showing a Cre-out strategy. **(B-D)** Ca^{2+} activity time-locked to each attack episode. The panels showing (B) Distribution of attack episode, (C) Heatmap of GCaMP6m, and (D) ΔF/F%. **(E)** Analysis of peak ΔF/F before (Pre) and after (Post) each attack episode. Data represent mean ± S.E.M. Significance was calculated by means of unpaired *t*-test. $^*P < 0.05$. **(F)** Analysis of peak ΔF/F in $dmPAG^{Tac2}$ neurons (N = 10 trails, in Figure 3H) versus $dmPAG^{Tac2}$ negative neurons (N = 46 trails) during each attack episode. Data represent mean ± S.E.M. Paired *t*-test, $^{****}P < 0.0001$.

Figure S4. **Tac2-expressing neurons in dmPAG respond to aggression** (related to Figure 3)

(A-F) Ca^{2+} activity time-locked to male-male encounter (A-B), male-female encounter (C-D), and male-female interaction (E-F). (A) Heatmap of GCaMP6m ΔF/F signals (top) and ΔF/F% (bottom). (B) Analysis of peak ΔF/F before (Pre) and after (Post) each male-male encounter episode. The other panels present the same manner but with different behavioral events, including male-female encounter (C-D) and male-female interaction (E-F). **(G-H)** Ca^{2+} activity time-locked to motor activity in the rotarod test. (G) heatmaps of GCaMP6m ΔF/F signals (top) and ΔF/F% (bottom). (H) Analysis of peak ΔF/F before (Pre) and after (Post) the start of rotarod test. **(I-P)** Ca^{2+} activity time-locked to object exploration (I-J), fox odor sniffing (K-L), saline odor sniffing (M-N), and pain stimulation (O-P). (I) Distribution of object exploration (top), heatmaps of GCaMP6m ΔF/F signals (middle) and ΔF/F% (bottom). (J) Analysis of peak ΔF/F before (Pre) and after (Post) each object exploration episode. The other panels present the same manner but with different behavioral events, including fox odor sniffing (K-L), saline odor sniffing (M-N), and pain stimulation (O-P). Data represent mean ± S.E.M. Significance was calculated by means of paired *t*-test.

Figure S5. Behavioral phenotypes (locomotion, anxiety, social behaviors) in *Tac2*-Cre mice (related to Figure 4).

(A) Schematic of the open-field test. **(B-E)** Locomotor performance of WT and *Tac2*-Cre mice on (B) total

distance, (C) average speed, (D) time spent in central and peripheral zones, and (E) entries into the central and peripheral zones. **(F)** Schematic of the elevated-plus maze test. **(G-J)** Anxiety-like behaviors of WT and *Tac2*-Cre mice on (G) numbers of entries in closed arm, (H) time spent in closed arm, (I) numbers of entries in open arm, (J) time spent in open arm. **(K)** Schematic of the social interaction test (sociability session). **(L-M)** Social preference of WT and *Tac2*-Cre mice on (L) interaction time and (M) social preference index. **(N)** Schematic of the social interaction test (social novelty session). **(O-P)** Social preference of WT and *Tac2*-Cre mice on (O) interaction time and (P) social preference index. **(Q)** Schematic of the RI assay. **(R-T)** Behavioral performance of WT and *Tac2*-Cre mice on (R) latency to attacks, (S) number of attacks and (T) duration of attacks. Data represent mean ± S.E.M. N = 24 in WT mice and N = 25 in *Tac2*-Cre mice. Unpaired t-test, * $P < 0.05$, *** $P < 0.001$, **** $P < 0.0001$.

Figure S6. Percentage of *Tac2*-Cre mice exhibit attack behaviors (related to Figure 4-5).

(A) Percent of mice exhibiting attack before and after genetic ablation with DTA or mCherry (control). (**B**) Number and duration of investigation before and after ablation of dmPAG^{Tac2} neurons with DTA. N = 7/group. **(C)** Percent of mice exhibiting attack before and after receiving hM4Di or mCherry (control). **(D)** Percent of animals exhibiting attack before and after hM3Dq or mCherry (control). Data represent mean ± S.E.M. Significance was calculated by One-way ANOVA and Tukey's multiple comparisons test,

Figure S7. **Behavioral phenotypes (locomotion and anxiety behaviors) following chemogenetic inhibition** (related to Figure 4).

(A-D) Performance of the open-field test in *Tac2*^{hM4Di} mice receiving saline or CNO (1 mg/kg, *i.p.*). Analysis showing results of total distance (A), average speed (B), time spent in the central or peripheral zones (C), and entries into the central or peripheral zones (D). **(E-H)** Performance of the elevated-plus maze in *Tac2*^{hM4Di} mice receiving saline or CNO (1 mg/kg, *i.p.*). Analysis showing results of entries in the open arm **(E)**, total time spent in the open arm **(F)**, entries in the closed arm **(G)**, and total time spent in the closed arm **(H)**. N = 10 mice/group. Data represent mean ± S.E.M. Significance was calculated by means of paired *t*-test, *$P < 0.05$.

Figure S8. **Behavioral phenotypes (locomotion and anxiety behaviors) following chemogenetic activation** (related to Figure 5).

(A-D) Performance of the open-field test of *Tac2*^{hM3Dq} mice receiving saline or CNO (0.5 mg/kg, *i.p.*). Analysis showing results of total distance (A), average speed (B), total time in the central or peripheral zones (C), and entries in the central or peripheral zones (D). **(E-H)** Performance of elevated-plus maze of *Tac2*^{hM3Dq} mice receiving saline or CNO (0.5 mg/kg, *i.p.*). Analysis showing results of entries in the open arm **(E)**, total time spent in the open arm **(F)**, entries in the closed arm **(G)**, and total time spent in the closed arm **(H)**. N = 8 mice/group. Data represent mean ± S.E.M. Significance was calculated by means of paired *t*-test.

<u>Figure S9</u>: **Pharmacological validation of molecular targets identified by TRAP-seq** (related to Figure 7)

(A). Heatmap showing counts of *Tph2* from TRAP-seq raw results. **(B)** Heatmap showing Log_2FC value of *Tph2* transcript counts in individual sample pairs. **(C)** Counts of 5-HT system-related genes detected in the IP samples from RI mice and home-cage controls. **(D)** Log_2FC value in the counts of 5-HT system-related genes in the IP samples from RI mice normalized to that of the home-cage control mice.